Spectrochimica Acta Part A: Molecular and Biomolecular Spectroscopy 315 (2024) 124227

Contents lists available at ScienceDirect

Spectrochimica Acta Part A:
Molecular and Biomolecular Spectroscopy

journal homepage: www.journals.elsevier.com/spectrochimica-acta-part-a-molecular-and-biomolecular-spectroscopy

Dicyanopyridine derivatives: One-pot preparation, ACQ-to-AIE transformation, light-conversion quality and photostability

Yanjin He [a,1], Jiaqi Liu [b,1], Chenwei Hu [b], Yongtao Wang [a,*], Lei Ma [b,*], Yanjun Guo [a]

[a] Guangxi Key Laboratory of Electrochemical and Magneto-chemical Function Materia, College of Chemistry and Bioengineering, Guilin University of Technology, Guilin 541004, China
[b] Tianjin International Center for Nanoparticles and Nanosystem, Tianjin University, Tianjin 300072, China

HIGHLIGHTS

- The ACQ-to-AIE transformation was successfully realized.
- The mechanism of ACQ-to-AIE transformation was discussed in detail.
- AIE-active DCC can be prepared in large scale and high-yield.
- DCC shows the matching fluorescence peak with crop absorption.
- DCC shows excellent photostability in doping film.

GRAPHICAL ABSTRACT

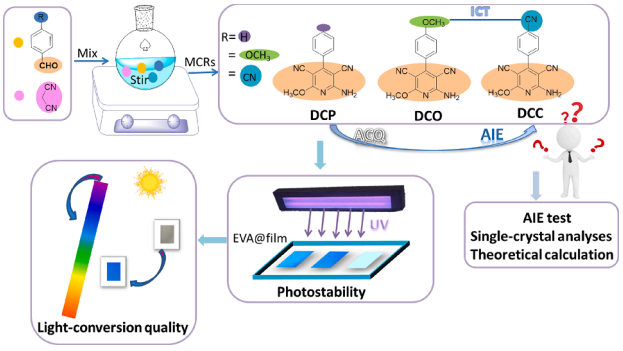

ARTICLE INFO

Keywords:
Aggregation-induced emission
ACQ-to-AIE transformation
Light conversion agent
Light conversion film
Dicyanopyridine derivatives

ABSTRACT

Low cost and strong fluorescence emission are two important guarantees for luminogens used as light conversion agents. By one-pot multicomponent approach and inexpensive starting materials, three dicyanopyridine (DP) derivatives named as DCP (2-amino-6-methoxy-4-phenylpyridine-3,5-dicarbonitrile), DCO (2-amino-6-methoxy-4-(4-methoxyphenyl) pyridine-3,5-dicarbonitrile) and DCC (2-amino-4-(4-cyanophenyl)-6-methoxypyridine-3,5-dicarbonitrile) were designed and synthesized.

Meanwhile, the ACQ-to-AIE transformation was successfully realized by altering substituent groups rather than traditional rotor–stator theory. Based on crystal analysis and theoretical calculations, the ACQ-to-AIE transformation is attributed to the tunable stacking modes and intermolecular weak interactions. Owing to matched fluorescence emission, low lost, high yield, and AIE activity, DCC is used as light conversion agents and doped in EVA matrix. The light conversion quality confirms that DCC can not only convert ultraviolet light, but also significantly improve the transmittance of 25 %/40 % EVA, whose photosynthetic photon flux density at 400–500 nm and 600–700 nm increased to 30.67 %/30.21 % and 25.37 %/37.82 % of the blank film, respectively. After 20 h of UV irradiation (365 nm, 40 W), the fluorescence intensities of DCC films can maintain 92 % of the initial values, indicating good photostability in the doping films. This work not only provides an excellent

* Corresponding authors.
E-mail addresses: wyt_shzu@163.com (Y. Wang), lei.ma@tju.edu.cn (L. Ma).
[1] Contributed equally.

https://doi.org/10.1016/j.saa.2024.124227
Received 30 December 2023; Received in revised form 11 March 2024; Accepted 29 March 2024
Available online 2 April 2024

and low-cost light conversion agent, but also has important significance for ACQ-to-AIE transformation of luminogens.

1. Introduction

The study found that α-Carotene, lutein, chlorophyll *a* and chlorophyll *b* play a decisive role in photosynthesis of plants [1–4]. Furthermore, α-Carotene and lutein have strong absorption in the blue-violet light (430–480 nm) region, and chlorophyll *a* and chlorophyll *b* have two strong absorption bands in the blue-violet light (430–480 nm) and red light (600–700 nm) regions [5–13]. Thereby, we know that not all sunlight is beneficial for plant photosynthesis. Among of sunlight, the ultraviolet light below 380 nm is harmful to crop growth, while the green light at 500–580 nm is basically not absorbed [14,15]. Based on the theory of photoecology and light conversion effects, light conversion agent can convert ultraviolet light and yellow-green light into blue-violet light and red–orange light required for plant photosynthesis, which not only reduces plant diseases and insect pests, but also boosts crop growth, improves crop quality and shortens crop growth cycle [16–21]. The main evaluation criteria of light conversion agents include excellent spectral matching, persistent photostability, high transmittance, good compatibility and low cost [22]. At present, among all kinds of light conversion agents, inorganic salt light conversion agents have good high-temperature resistance and are easy to prepare and store, but their compatibility with organic film resin is poor, and their crystallinity is high, which easily leads to uneven dispersion and poor transmittance. Organic complexes have high luminous efficiency, good photothermal stability, and good compatibility with polymer matrix, but whose disadvantages lie in narrow convertible spectra, cumbersome preparation, and high costs. Owing to good resin compatibility and adjustable emission wavelength, organic fluorescent dyes have attracted more and more attention as light conversion agents [23–26]. However, large scale applications of organic fluorescent dyes are still limited due to complex preparation process, high costs, and easy photobleaching/photodegradation [22,27].

To solve the above problems, it is urgent to seek and design luminogens with short synthesis routes, high yield, and aggregation induced emission (AIE) characteristic [28,29]. On the one side, developing simpler methods to prepare light conversion agents is one of the key research areas in the entire field of light conversion films. Multicomponent reactions (MCRs) have been widely used in the synthesis of bioactive compounds in heterocyclic, pharmaceutical, and combinatorial chemistry due to their advantages such as short reaction time, high yield, and simple treatment procedures [30–32]. In the past decade, multi-component reactions have been considered an important tool in organic chemistry because they can synthesize novel small molecular materials with excellent application performance. More importantly, the short synthesis routes and high yield are beneficial to reduce the cost [33–35]. On the other side, AIE luminogens can emit strong fluorescence in the aggregated state, and thereby enhance light conversion efficiency. According to the reported literatures [36–38], some 3, 5-dicyanopyridine (DP) derivatives can be constructed by one-pot multicomponent approach and inexpensive starting materials, but it still needs some harsh reaction conditions due to the presence of sodium methoxide[39]. Moreover, DP derivatives are typically used as a corrosion inhibitor and drug, but the corresponding optical performance is rarely explored. Generally, AIE luminogens are constructed based on the concept of rotor and stator, whose propeller-like or twisted molecular configurations can suppress intermolecular π-π interactions, thereby avoiding aggregation induced quenching (ACQ) [40]. Different from traditional concept of rotor and stator, changing electronic effect of substituent groups can adjust intramolecular charge transfer and further trigger different intermolecular stacking mode in theory, thus achieving a transformation between ACQ and AIE [41–44]. It is worth mentioning that introducing different substituent groups is a faster and convenient mode compared with traditional rotor and stator. However, this ACQ-to-AIE transformation mode was rarely reported before.

As shown in Scheme 1, here highly substituted pyridine derivatives, named DCP with neutral functional group (H), DCO with electron-donating functional group (-OMe), and DCC with electron-withdrawing functional group (–CN) were obtained through an efficient one-pot multicomponent reaction [39,45,46]. The synthesis process uses aqueous sodium hydroxide solution instead of sodium methoxide, and it can be found to have the characteristics of simple synthesis steps, low cost, and high yield. From electron donating substituents (OMe) to hydrogen, to electron withdrawing substituents (CN) [47], ACQ-to-AIE transformation is successfully realized, which is mainly attributed to different intermolecular interactions and the resulting distinct intermolecular stacking modes. By selecting 25 % ethylene vinyl alcohol copolymer (EVA, polyvinyl alcohol accounts for 25 % of the weight of the EVA copolymer) and 40 % EVA (polyvinyl alcohol accounts for 40 % of the weight of the EVA copolymer) as the doping matrix, various doped films were prepared [48–50]. Taking advantage of strong intramolecular and intermolecular hydrogen bonds of EVA, the diffusion of oxygen into the light conversion film can be effectively inhibited, and thereby yielding excellent photostability [51,52]. Crystal analysis combined with theoretical calculations, as well the tests of absorption spectra, emission spectra, AIE activity, photostability, and light conversion quality, luminescence performance and the corresponding intrinsic mechanism were discussed in detail.

2. Experimental section

2.1. Measurement and characterization

^{1}H NMR spectra and ^{13}C NMR spectra were obtained with a Varianinova instrument at 500 MHz and 100 MHz using tetramethylsilane (TMS) as the internal standard, and DMSO as the solvent in all cases. UV–vis absorption spectra were obtained on a MaPada UV-3200PCS spectrophotometer. Fluorescent emission spectra were obtained on a Hitachi F-2500 fluorescence spectrophotometer. MALDI/HRMS was recorded on an UltrafleXtreme MALDI-TOF/TOF mass spectrometer (Bruker, Germany). Single-crystal X-ray diffraction data were collected by Oxford Diffraction Xcalibur Eos diffractometer equipped with an Eos detector and operating graphite monochromated MoKα radiation (λ = 0.71073 Å). Thermal stability was determined by thermogravimetric analyzer (TGA, SDT Q600) over a temperature range of 20–1000 °C at a heating rate of 10 °C min^{-1} under N_2 atmosphere.

2.2. Materials

All the chemicals and reagents used in this study were of analytical grade without further purification. In general, all the intermediates and final compounds were purified by column chromatography on silica gel (200–300 mesh), and crystallization from analytical grade solvents. Reactions were monitored using thin layer chromatography (TLC). The synthetic methods of target compounds were shown as Scheme 1.

2.3. Synthesis procedures

2.3.1. 2-amino-6-methoxy-4-phenylpyridine-3,5-dicarbonitrile (DCP)

To a stirred mixture of benzaldehyde (3.0 mmol) and malononitrile (6.0 mmol) in aqueous methanol (60 %, 20 mL), sodium hydroxide (3.5 mmol) was added at room temperature. After the reaction was completed as monitored by TLC using ethyl acetate: hexanes 1:2, the

precipitate of desired products was filtered, dried, and recrystallized from methanol. A yellow solid was obtained in yield of 84 %. mp 251.2–251.9 °C. ^{1}H NMR (500 MHz, DMSO-d_6) δ 8.16 (s, 2H), 7.54–7.45 (m, 5H), 3.93 (s, 3H) (Fig.S1†). ^{13}C NMR (100 MHz, DMSO-d_6) δ 166.23, 161.64, 161.24, 134.59, 130.75, 129.14, 128.82, 115.92, 115.50, 83.88, 83.71, 55.22 (Fig.S2†). HRMS (MALDI-TOF): *m/z* 273.0749 [[M + Na] $^{+}$, calculated 273.0747] (Fig. S3†).

2.3.2. 2-amino-6-methoxy-4-(4-methoxyphenyl) pyridine-3,5-dicarbonitrile (DCO)

A yellow solid (2.64 g) was obtained in 87 % yield. mp 233.2–233.7 °C. ^{1}H NMR (500 MHz, DMSO-d_6) δ 7.93 (s, 2H), 7.48 (d, J = 9.7 Hz, 2H), 7.12 (d, J = 8.7 Hz, 2H), 3.97 (s, 3H), 3.85 (s, 3H) (Fig. S4†). ^{13}C NMR (100 MHz, DMSO-d_6) δ 166.36, 162.39, 161.24, 160.92, 130.23, 126.51, 117.32, 115.76, 114.52, 85.04, 55.82, 55.17 (Fig.S5†). HRMS (MALDI-TOF): *m/z* 303.0853 [[M + Na] $^{+}$, calculated 303.0853] (Fig. S6†).

2.3.3. 2-amino-4-(4-cyanophenyl)-6-methoxypyridine-3,5-dicarbonitrile (DCC)

2.58 g of yellow solid was obtained in 83 % yield. mp 262.5–263.4 °C. ^{1}H NMR (500 MHz, DMSO-d_6) δ 8.27 (s, 1H), 8.08 (d, J = 8.2 Hz, 4H), 7.76 (d, J = 8.3 Hz, 4H), 7.35 (s, 1H), 4.12 (s, 1H), 3.98 (s, 7H) (Fig.S7†). ^{13}C NMR (100 MHz, DMSO-d_6) δ 166.64, 162.71, 158.73, 140.82, 133.58, 130.02, 117.89, 116.33, 115.17, 112.21, 83.74, 81.88, 54.51 (Fig.S8†). HRMS (MALDI-TOF): *m/z* 298.0698 [[M + Na] $^{+}$, calculated 298.0700] (Fig. S9†).

2.4. Preparation of light conversion films

Dissolve 25 % EVA (defined as EVAa) /40 % EVA (defined as EVAb) (1 g) and DCP (0.01 g) in a round bottom flask with 15 mL THF, then place in an ultrasonic oscillator for 3 h, and mix evenly. Pour the mixture onto a glass plate and spread it quickly with a glass rod. Finally, put the film into a fume hood until THF is completely volatilized to obtain corresponding DCP (1 % mass fraction) light conversion films, named DCP@EVAa/DCP@EVAb film. According to this method, other light conversion films were obtained.

3. Results and discussion

3.1. Preparation and photo-physical properties in solution

As shown in Scheme 2, preparation of DCP, DCO and DCC went through five intermediate processes. The yields of three compounds are basically the same, indicating that the electronic effects of OMe and CN groups did not affect the reaction process. For DCP, ^{1}H NMR spectrum showed the presence of a singlet signal at δ 3.93 characteristic of OCH_3 group. It also exhibited a doublet signal at δ 7.50 for five aromatic protons and a singlet signal at δ 8.16 for the amino group (Fig. S1). Meanwhile, ^{13}C NMR spectrum of DCP exhibited signals of the methoxy and nitrile carbons at δ 55.22, 115.50, 115.92 in turn, while the pyridine C-3 and C-5 appeared at δ 83.71 and 83.88 (Fig. S2). DCO and DCC provided similar structural features, and molecular structures of DCP and DCC were further confirmed by single crystal diffraction. The UV–vis absorption and fluorescence spectra of DCP, DCO and DCC in various organic solvents (1×10^{-5} mol/L) were investigated, as shown in Fig. 1 and Table S1†. The three dyes have two strong absorption bands at 230–300 nm and 300–400 nm, which are attributed to π-π* transitions and intramolecular charge transfer (ICT) states, respectively. With the increase of the polarity of the solvents, the absorption maxima of the three dyes change slightly, but their emission maxima continue to red shift from Tol, DCM to DMSO, which is due to be a larger dipole moment in the excited state relative to the ground state. In the same solvent, it is noteworthy that emission maxima gradually redshift from DCP, DCO to DCC, which may be related to enhanced ICT effect in turn. Besides, DCP and DCO show the maximum absorption wavelength in Tol, illustrating stronger conjugation for two luminogens in Tol than DCM and DMSO, but for DCC in DMSO rather than Tol [53], which is plausible to associate the above phenomenon with different electronic effects of substituents, although fully understanding the exact mechanism remains a challenge. The relative fluorescence quantum yields (PLQYs) of DCP, DCO and DCC were determined in Tol, DCM and DMSO by using quinine sulphate as the reference, and the resulting photophysical parameters were listed in Table S1. Overall, PLQYs of three compounds are not high in solution, which may be due to the rotational and vibration between the pyridine ring and the benzene ring.

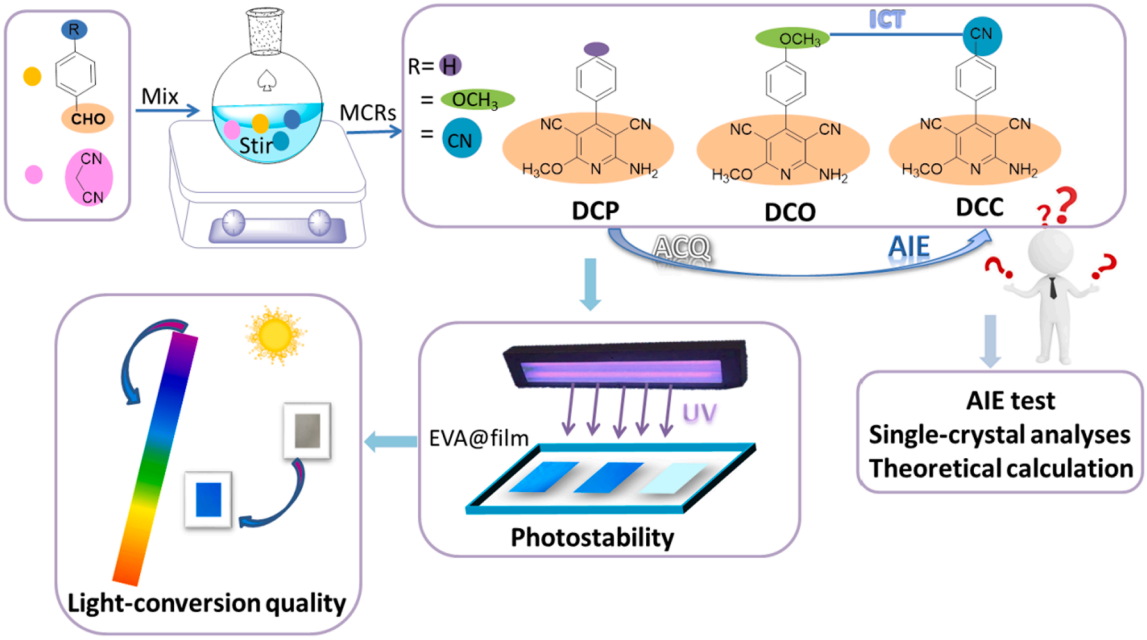

Scheme 1. Synthesis, ACQ-to-AIE transformation, mechanism, and application of dicyanopyridine derivatives.

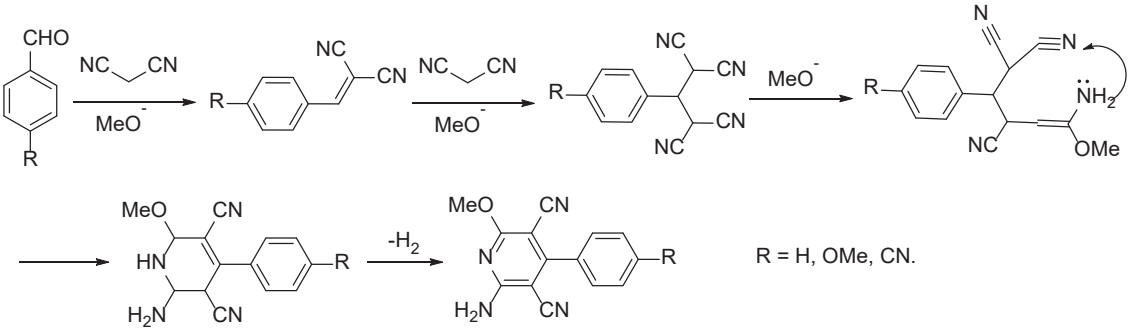

Scheme 2. The reaction mechanism of DCP, DCO and DCC.

3.2. Aggregation-induced emission

To investigate the emission characteristics of DCP, DCO and DCC, the fluorescence emission spectra of three dyes were tested in THF-H_2O mixed solution with different water fractions (f_w, from 0 % to 90 %, v/v). Fig. 2 shows the fluorescence intensities of DCP and DCO decrease rapidly with the increase of f_w, confirming obvious ACQ effect. Different from DCP and DCO, DCC shows apparent AIE behavior, whose fluorescence intensity gradually enhances as f_w increases from 0 % to 40 % and from 50 % to 90 %. To further explore the internal mechanism of ACQ and AIE behavior, emission maxima of three dyes were also analyzed. When f_w increases 20 %, emission maxima of DCP shows obvious blue shift, and then present continuous shocks, which is difficult to give a clear explanation for the above phenomenon by the change of solvent polarity and the formation of aggregated state. Different from DCP, emission maxima of DCO continues to redshift with the increase of f_w from 0 to 70 %. Subsequently, rapid blueshift can be observed at f_w from 80 % to 90 %. As speculation, the former may be due to the increased solvent polarity, resulting in the enhancement of ICT effect, while the latter should be attributed to aggregated state. Interestingly, emission maxima of DCC firstly red shift as f_w increases from 0 % to 40 %, which may be due to the increase of solvent polarity. Then emission maxima blue shift sharply, suggesting the formation of aggregated state [54,55]. The similar molecular structure yields significantly different optical properties, which should be attributed to the push–pull electronic ability of the substituent group (OCH_3 and CN) and different intermolecular stacking modes. The further intrinsic mechanism needs to be discussed by crystal analysis and theoretical calculation.

3.3. Single-crystal analyses

To ascertain the internal mechanism of ACQ-to-AIE transformation, DCP (CCDC 2268953) and DCC (CCDC 2268954) crystals are analyzed, as shown in Fig. 3. crystal DCP is a triclinic system with the space group P-1, in the unit cell two molecules adopts head to tail antiparallel stacking mode. There is a strong tendency to establish π-π stacking interactions between pyridine units, whose plane to plane (C_p-C_p) and centroid to centroid (C_g-C_g) distances are 3.647 Å and 3.909 Å respectively. It is widely known that that π-π stacking often causes fluorescence reduction or quenching, which is consistent with the ACQ characteristics of DCP. Furthermore, DCP shows distorted molecular configurations with and dihedral angle of 58.89° between benzene ring and pyridine unit, and neighboring molecule generate varied intermolecular hydrogen bonds and weak intermolecular interactions. By contrast, DCC has very different molecular packing from DCP, in the unit cell four molecules divided into two groups adopt antiparallel stacking modes, but no π-π stacking interactions are found. Compared with DCP, DCC show more and stronger (2.254 and 2.333 Å) intermolecular hydrogen bonds and weak intermolecular interactions, and twist of molecular configuration slightly increased, whose dihedral angle between benzene ring and pyridine unit increases to 59.17°. Thereby, strong intermolecular interactions and lack of π-π stacking can be responsible for AIE behavior of DCC, while similar molecular conformations are independent of ACQ-to-AIE transformation.

3.4. Theoretical calculation

To further explain the inherent mechanism of ACQ-to-AIE transformation, theoretical calculation of DCP and DCC were accomplished by extracting single crystal structures, which were fully reoptimized by employing Gaussian16 program package at PBE-def2svp level. The corresponding excited state and energy calculations were performed at PBE0-def2tzvp level and optimized by using dispersion correction. For comparison, ground state and excited state of DCP and DCC monomer were firstly investigated (Table 1 and Fig. 4). The results show that DCP and DCC have similar molecular configuration, whose dihedral angles between ring A and B are about 55° in the ground state. When molecule transitions to the excited state from the ground state, DCP and DCC present more planar molecular configuration. The dihedral angle of ring A-B is reduced to 40° and 0° for DCC and DCP respectively, meanwhile, B ring of DCP gives 25° bending. Furthermore, both DCP and DCC show intramolecular charge transfer characteristics, and electron density distribution of the highest occupied molecular orbital (HOMO) is mainly concentrated on B-ring of DCC and DCP, but electron density distribution of the lower unoccupied molecular orbital (LUMO) is distributed over the whole molecule of DCC and DCP (Fig. 4b). The aggregated state molecule models of DCC and DCP were established by using the OMION method. As shown in Fig. S10, the dimer in the 3*3 supercell center are selected as the upper layer, which is optimized by adopting PBE-def2svp basis set, and the excited state calculations are performed with PBE0 functional and def2tzvp basis set, while the remaining molecules are used as lower layers to freeze atomic coordinates, and the force fields of all atoms are fitted by using universal UFF method. The results showed that DCC and DCP molecules yield tiny conformational deformation from the ground state to the excited state, but their stacking modes present significant differences (Fig. S11). By comparison, DCP shows closer molecular stacking, whose centroid distances are 4.62 Å and 4.90 Å respectively from ground state to the excited state, while the corresponding centroid distance increases to 6.61 Å from 6.02 Å for DCC. Subsequently, intermolecular noncovalent interactions were carried out by interaction region indicator (IRI) analysis. The blue, green and red regions represent intermolecular strong, hydrogen bonding and weak interactions, and potential resistance in turn, and all isosurfaces were set to 1. As shown in Fig. 5, red area is absent in the calculation, and the blue regions are all located at the bonding site, while the green area is located between the surfaces of two face to face molecules. Compared with DCC, wider green areas can be observed in DCP dimer due to intermolecular π-π stacking occurring on DCP instead of DCC. Owing to intermolecular π-π stacking, the oscillator intensity (*f*) of DCP significantly decreases from molecule monomer to aggregated state, corresponding to ACQ characteristic of DCP. For DCC, the aggregation-induced enhancement activity was not found in the calculation, whose

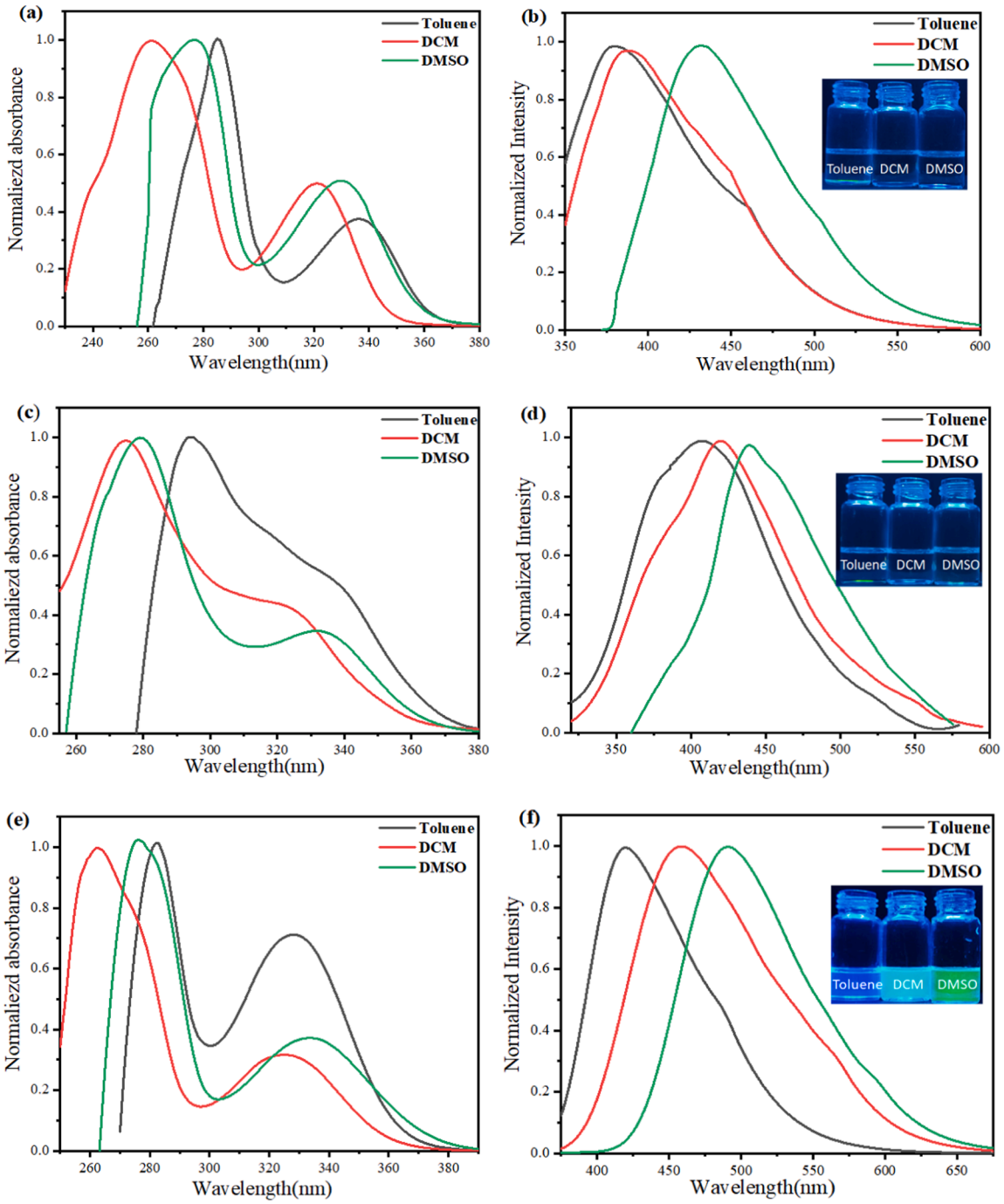

Fig. 1. Normalized UV–vis absorption spectra of (a) DCP, (c) DCO and (e) DCC in various solvents (solution concentration: 10 μM). Normalized fluorescence spectra of (b) DCP, (d) DCO and (f) DCC in various solvents (solution concentration: 10 μM, inset is the irradiation of different solvents under 365 nm UV illumination).

f dropped to 0.059 from 0.097 rather than increased possibly due to the existence of weak interactions between DCC molecules in the above calculation model (Table 1). Even so, the above-mentioned theoretical calculation methods are expected to be used to predict fluorescence emission trend of the same series luminogens from single molecule to aggregated state.

3.5. Light-conversion quality

The doped films were prepared by dissolving DCP/DCO/DCC and EVAa/EVAb at a weight ratio of 1:100. For convenience of description, DCP@EVAa and DCP@EVAb are defined according to the light conversion agent and doped matrix. Based on the above rule, other doped films are named as DCO@EVAa, DCC@EVAa, DCO@EVAb and DCC@EVAb in turn. Under UV radiation, DCP@EVAa and DCP@EVAb films emit deep blue fluorescence, whose emission wavelengths are 417 nm and 400 nm respectively (Fig. 6 and Table S4†). Obviously, DCP is not suitable for use as a light conversion agent due to short emission wavelength. Interestingly, both DCO with electron donating group (OMe) and DCC electron withdrawing group (CN) exhibit bathochromic-shift fluorescence emission. Moreover, emission maxima of DCO and DCC match with the absorption maxima of chlorophyll *a* and b very well in doping film. Furthermore, the light conversion quality of the doping films is measured and evaluated by using the HiPoint HR-450 analyzer, and the blank film without dye was chosen as a control. Fig. 6 shows DCC@EVAa and DCC@EVAb have the highest spectral intensity, while

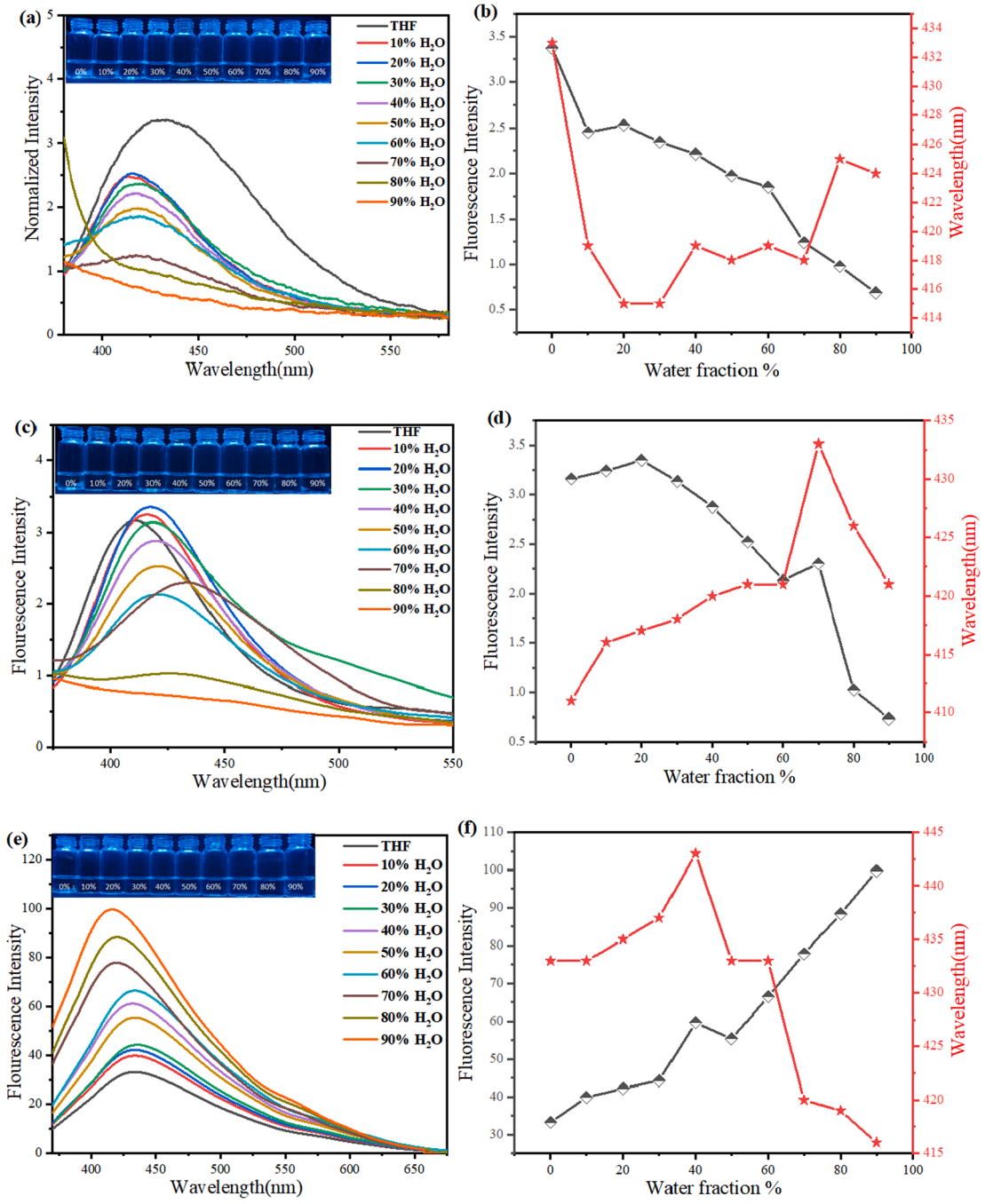

Fig. 2. Fluorescence emission spectra of (a) DCP, (c) DCO and (e) DCC in THF-H_2O mixtures with different water contents (solution concentration: 10 μM). Fluorescence intensity at emission peak, emission maxima and water fraction of (b) DCP, (d) DCO and (f) DCC. Solution concentration: 10 μM. (inset: images in THF-water mixtures with different fractions of water under 365 nm UV illumination).

spectral intensity of DCO@EVAa and DCP@EVAa films increases slightly compared with that of blank film, which should be attributed to their AIE/ACQ characteristic. It is noteworthy that EVAb films exhibit higher spectral intensity and photon flux density (PFD) than the corresponding EVAa films, which should be because the increase of PVA units in EVAb is conducive to enhance transmittance of films and inhibit non-radiative energy loss of luminogens. Further research found that the spectral intensities of the DCC doped films were lower than that of the blank film before 400 nm, but they present significant enhancement compared to the blank film at 400–780 nm. In addition, not only did the blue-violet light (400–500 nm) significantly increase, but yellow green light (500–600 nm), red orange light (600–700 nm), and near-infrared light (700–780 nm) also significantly increased for DCC doped films than the blank film, indicating excellent ultraviolet light conversion performance and improved transmittance. More exactly, the photosynthetic photon flux density (PFD) of DCC@EVAa and DCC@EVAb films decreased by 5.51 % and 1.85 % compared to that of the blank film at 380–400 nm respectively, but their PFD increased by 30.67 %, 30.21 % and 25.37 %, 37.82 % at 400–500 nm and 600–700 nm in turn (Fig. 7 (b), (e) and Table S2†), indicating that DCC doped films have a significant improvement effect on blue-violet light and red orange light. It is worth mentioning that DCC doped films hardly change the ratio between blue-violet light and red orange light (Fig. 7 (c), (f) and Table S3†), which is also very important for the growth of many crops.

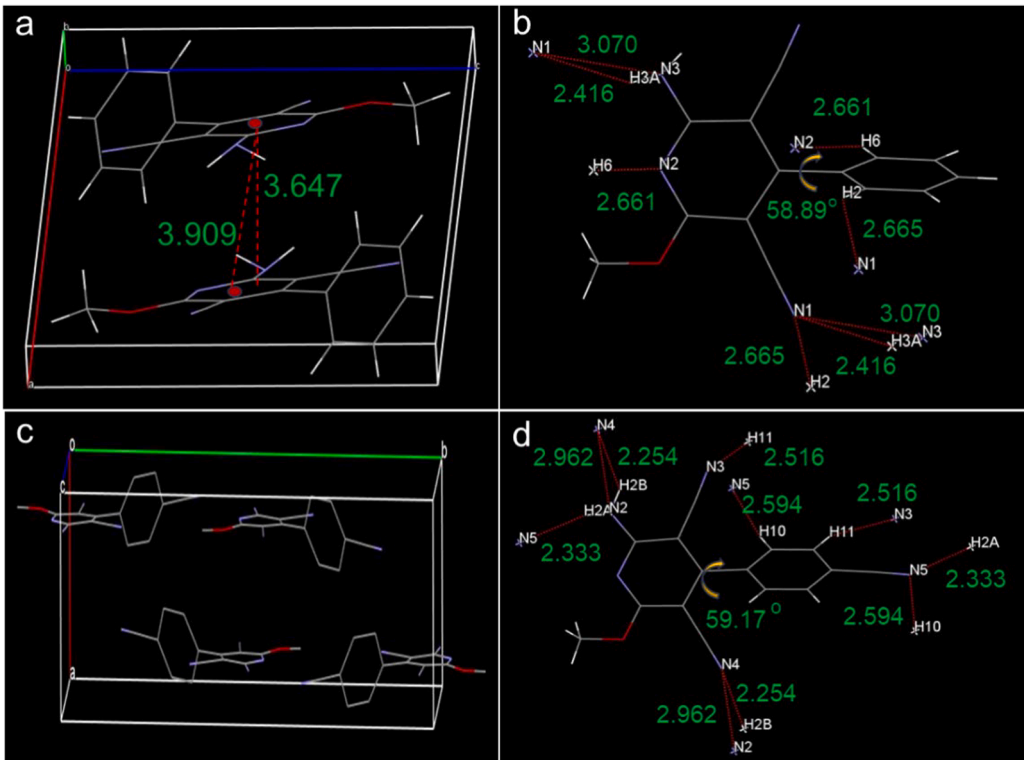

Fig. 3. Molecular stacking mode of (a) DCP, (c) DCC and single crystal structure (b) DCP, (d) DCC.

Table 1
Fluorescence absorption, emission energy and oscillator strength of DCP and DCC.

	E_{abs} (eV)[a]	f[b]	E_{em} (eV)[a]	f[b]
DCP monomer	4.017	0.143	2.128	0.064
DCC monomer	3.775	0.112	3.216	0.097
DCP dimer	4.248	0.000	3.057	0.003
DCC dimer	3.627	0.227	2.730	0.059

a E_{abs} = Fluorescence absorption energy; E_{em} = Fluorescence emission energy. b f = Oscillator strength.

3.6. Photostability and thermal stability

From the above, AIE-active DCC is the best light conversion agent. Next, its photostability are investigated by enhancing ultraviolet radiation (365 nm, 40 w). Fig. 8 shows that the fluorescence intensities of the three EVAa films can maintain 94.65 %, 89.42 %, and 91.95 % of the initial values after 20 h of UV irradiation, indicating that the dicyanopyridine derivatives have good photostability in the doping films. Compared with series EVAa, series EVAb have stronger fluorescence emission and smaller intensity fluctuation. We know that the polyvinyl alcohol unit in EVA copolymer can form strong intermolecular and intramolecular hydrogen bonds, inhibit non-radiative vibration and relaxation, and oxygen diffusion, thus improving the photostability and fluorescence intensity.

Excellent thermal stability is a very important evaluation index for light conversion agent; thereby thermogravimetric analysis (TGA) of DCC was performed. It can be seen from Fig. 9 that the thermal decomposition process of DCC can be divided into two stages. The first stage shows a slow slope line between 201 °C and 412 °C, according to the weight loss; –CN is removed in this stage. The second stage occurs between 412 °C and 683 °C, whose rapid decomposition should be the

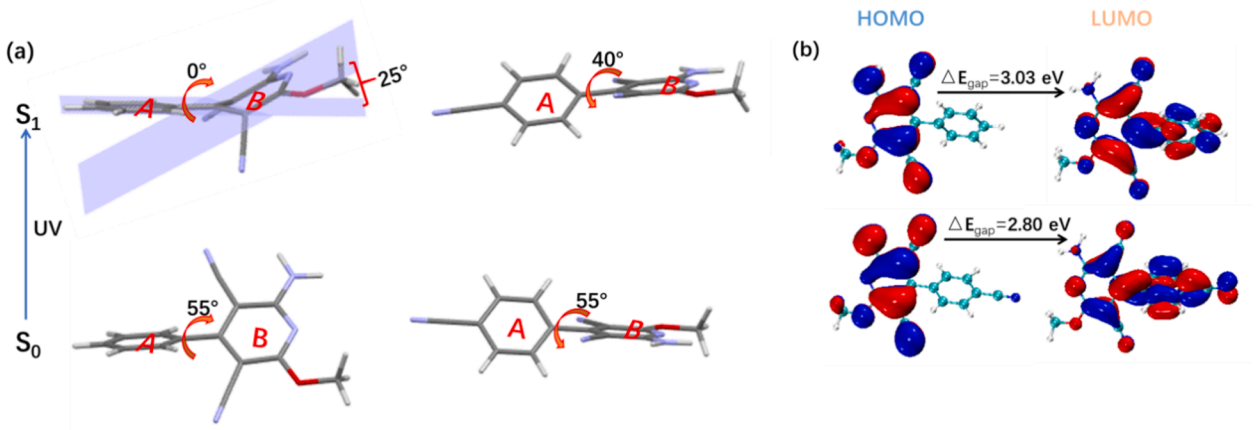

Fig. 4. (a) Molecular configuration of DCP and DCC on ground state and excited state; (b) HOMO and LUMO diagrams of DCP and DCC on ground state.

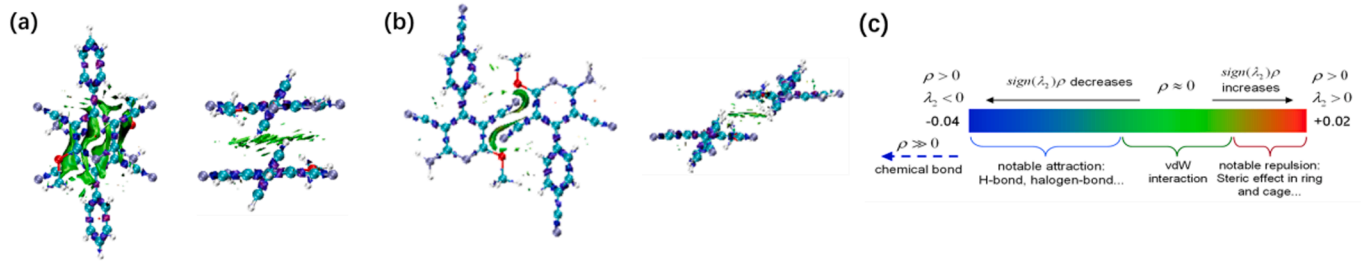

Fig. 5. Intermolecular noncovalent interactions analysis by IRI maps (a) DCP, (b) DCC and (c) IRI comparison chart.

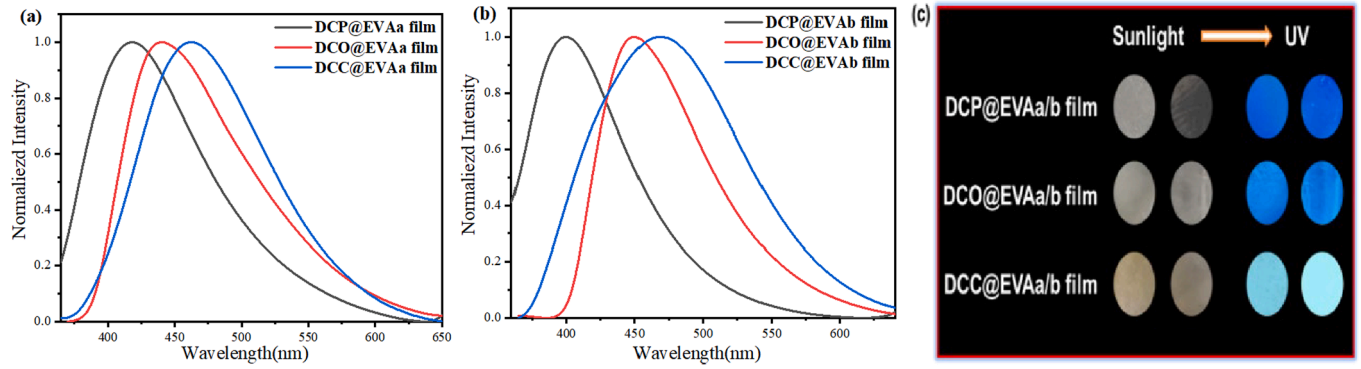

Fig. 6. Normalized emission spectra of (a) and (b) DCP, DCO and DCC@EVAa/EVAb films (doping mass fraction: 1%); (c) Images of different doped films under UV light.

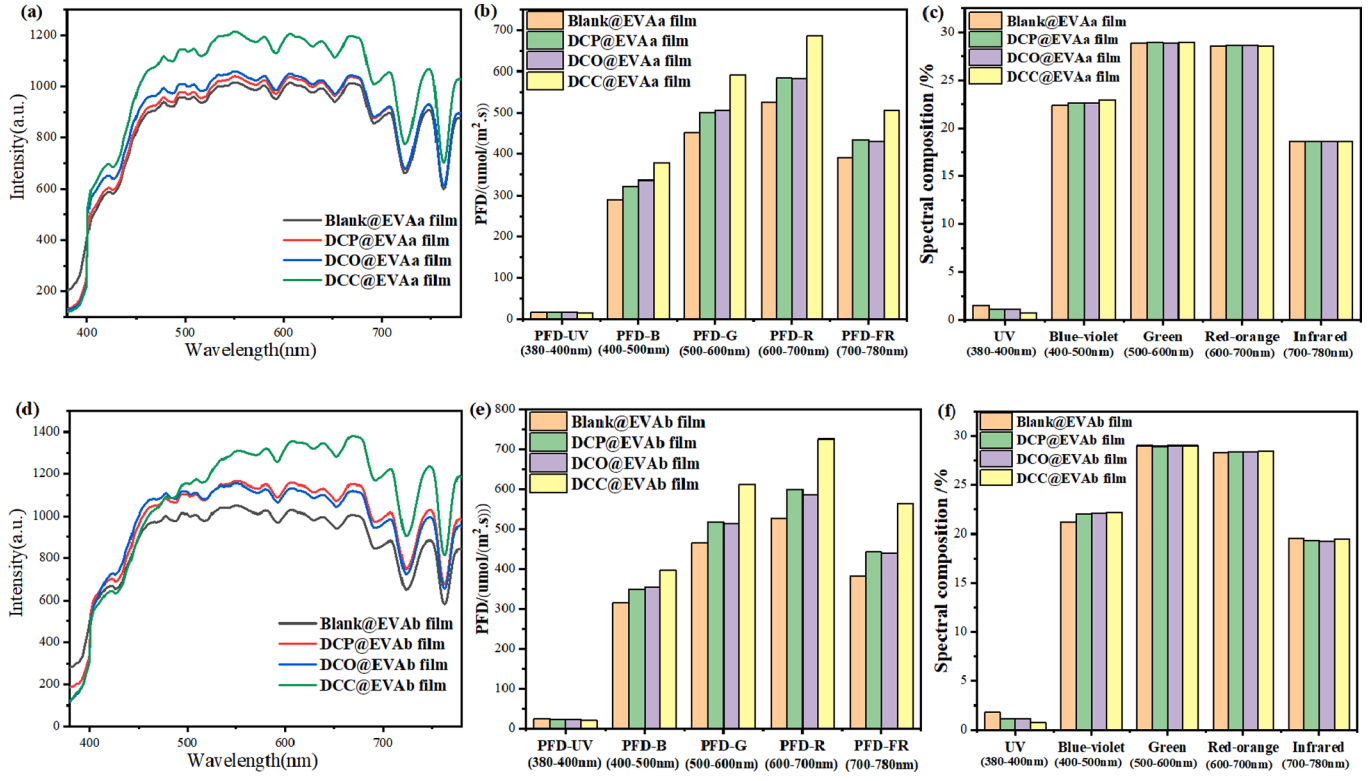

Fig. 7. (a), (d) Light quality measured under blank and DCP, DCO, DCC@EVAa/b films; (b), (e) PFD of UV, visible and infrared light of blank and DCP, DCO, DCC@EVAa/b films; (c), (f) UV, visible and infrared light compositions of blank and DCP, DCO, DCC@EVAa/b films.

result of decomposition, oxidation, and combustion. Overall, DCC can meet the application requirements of light conversion agent, and its initial decomposition temperature (T_d) is up to 281 °C (T_d is defined as the temperature at which the sample loses 5 % weight).

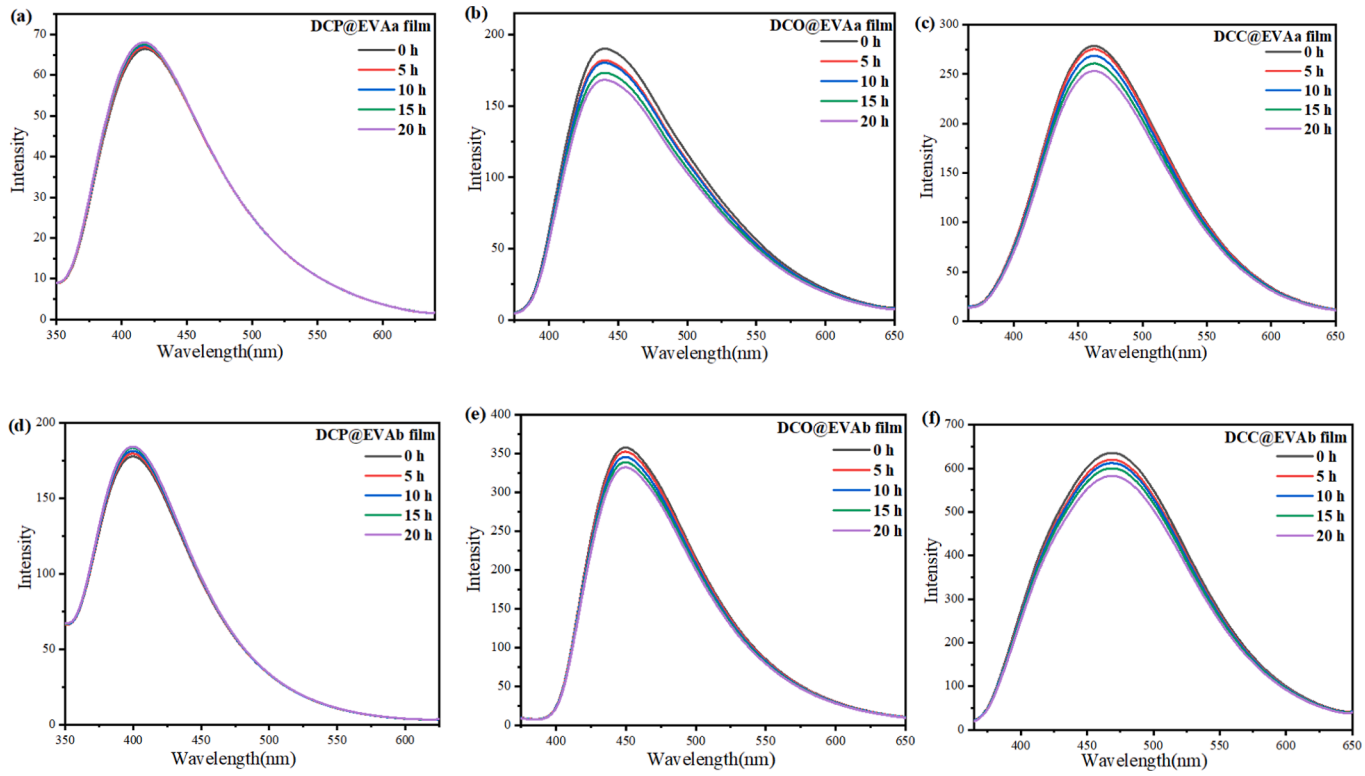

Fig. 8. Emission spectra of (a) DCP, (b) DCO, (c) DCC@EVAa films and (d) DCP, (e) DCO, (f) DCC@EVAb films at different radiation times.

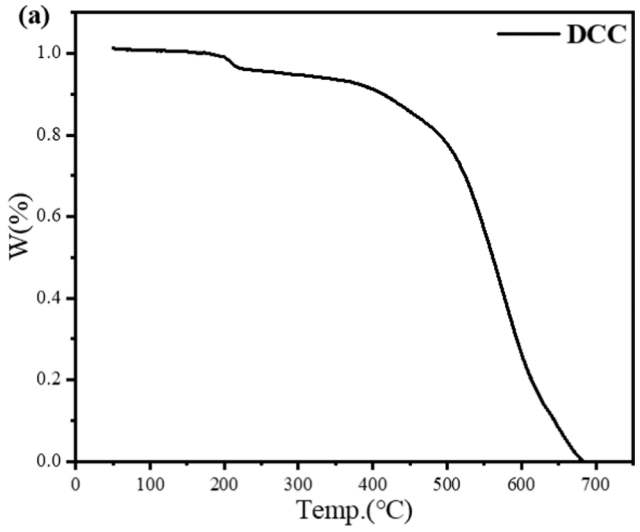

Fig. 9. TGA thermograms of (a) DCC recorded under nitrogen atmosphere at 10 °C min^{-1} scan rates.

4. Conclusion

In conclusion, three DP derivatives named as DCP, DCO and DCC were designed and synthesized by one-pot multicomponent approach, and they show obvious ICT effects in various solvents. By adjusting the electronic effect of substituents, the ACQ (DCP and DCO) to AIE (DCC) transformation was successfully realized. Crystal analysis and theoretical calculation indicate the ACQ-to-AIE transformation is attributed to different intermolecular stacking patterns. By contrast, DCC shows the strongest fluorescence emission and the best light conversion performance in doping films due to AIE activity. PFD of DCC@EVAa/EVAb films at 400–500 nm and 600–700 nm increased to 30.67 %/30.21 % and 25.37 %/37.82 % of the blank film, respectively. Obviously, DCC can not only convert ultraviolet light, but also significantly improve the transmittance of EVA films. More importantly, DCC exhibits excellent photostability and thermal stability in doping films, whose fluorescence intensities can maintain 92 % of the initial values after 20 h of UV irradiation (365 nm, 40 W), and its T_d is up to 281 °C. Based on the convenient preparation, high yield, AIE characteristic, matched fluorescence emission, excellent light conversion quality, as well outstanding photostability and thermal stability, DCC has the potential to become an excellent light conversion agent, while successful ACQ-to-AIE transformation by adjusting the electronic effect of substituents will provide a new way for construction of AIE materials. More importantly, fluorescence emission trend of luminogens from single molecule to aggregated state are expected to be predicted by the above-mentioned theoretical calculation model.

CRediT authorship contribution statement

Yanjin He: Writing – original draft. **Jiaqi Liu:** Data curation. **Chenwei Hu:** Data curation. **Yongtao Wang:** Writing – review & editing. **Lei Ma:** Validation. **Yanjun Guo:** Visualization.

Declaration of competing interest

The authors declare that they have no known competing financial interests or personal relationships that could have appeared to influence the work reported in this paper.

Data availability

Data will be made available on request.

Acknowledgment

This work was supported by the Guangxi Natural Science Foundation

(Grant No. 2020GXNSFAA159147), the National Natural Science Foundation of China (Grant No. 21766030 and 21566034) and the Guilin University of Technology Research Fund (Grant No. GUTQDJJ2019038 and GUTQDJJ2018052).

Appendix A. Supplementary material

Supplementary data to this article can be found online at https://doi.org/10.1016/j.saa.2024.124227.

References

[1] S. Streckaite, M.J. Llansola-Portoles, A.A. Pascal, C. Ilioaia, A. Gall, S. Seki, R. Fujii, B. Robert, Pigment structure in the light-harvesting protein of the siphonous green alga Codium fragile, Biochim. Biophys. Acta Bioenerg. 1862 (2021) 148384, https://doi.org/10.1016/j.bbabio.2021.148384.

[2] S. Banu, P.P. Yadav, Chlorophyll: the ubiquitous photocatalyst of nature and its potential as an organo-photocatalyst in organic syntheses, Org. Biomol. Chem. 20 (2022) 8584–8598. https://pubs.rsc.org/en/content/articlelanding/2022/ob/d2ob01473d.

[3] G. Gutierrez-Gamboa, S. Marin-San Roman, V. Jofre, P. Rubio-Breton, E.P. Perez-Alvarez, T. Garde-Cerdan, Effects on chlorophyll and carotenoid contents in different grape varieties (*Vitis vinifera* L.) after nitrogen and elicitor foliar applications to the vineyard, Food Chem. 269 (2018) 380–386, https://doi.org/10.1016/j.foodchem.2018.07.019.

[4] J.M. Artes Vivancos, I.H.M. Van Stokkum, F. Saccon, Y. Hontani, M. Kloz, A. Ruban, R. Van Grondelle, J.T.M. Kennis, Unraveling the excited-state dynamics and light-harvesting functions of xanthophylls in light-harvesting complex II using femtosecond stimulated Raman spectroscopy, J. Am. Chem. Soc. 142 (2020) 17346–17355. https://pubs.acs.org/doi/10.1021/jacs.0c04619.

[5] E.G. Nwoba, T. Rohani, M. Raeisossadati, A. Vadiveloo, P.A. Bahri, N. R. Moheimani, Monochromatic light filters to enhance biomass and carotenoid productivities of Dunaliella salina in raceway ponds, Bioresour. Technol. 340 (2021) 125689, https://doi.org/10.1016/j.biortech.2021.125689.

[6] S.A. Lohner, K. Biegert, A. Hohmann, R. Mccormick, A. Kienle, Chlorophyll- and anthocyanin-rich cell organelles affect light scattering in apple skin, Photochem. Photobiol. Sci. 21 (2022) 261–273. https://link.springer.com/article/10.1007/s43630-021-00164-1.

[7] K. Taulavuori, A. Pyysalo, E. Taulavuori, R. Julkunen-Tiitto, Responses of phenolic acid and flavonoid synthesis to blue and blue-violet light depends on plant species, Environ. Exp. Bot. 150 (2018) 183–187, https://doi.org/10.1016/j.envexpbot.2018.03.016.

[8] Y. Zhou, T. Seto, Z. Kang, Y. Wang, Design of highly efficient deep-red emission in the Mn4+ doped new-type structure CaMgAl10O17 for plant growth LED light, Dalton Trans. 50 (2021) 11793–11803. https://pubs.rsc.org/en/content/articlelanding/2021/dt/d1dt02088a.

[9] S. Fang, T. Lang, T. Han, M. Cai, S. Cao, L. Peng, B. Liu, Y. Zhong, A.N. Yakovlev, V. I. Korepanov, A novel efficient single-phase dual-emission phosphor with high resemblance to the photosynthetic spectrum of chlorophyll A and B, J. Mater. Chem. C 8 (2020) 6245–6253. https://pubs.rsc.org/en/content/articlelanding/2020/tc/d0tc00811g.

[10] M. Kosugi, S.I. Ozawa, Y. Takahashi, Y. Kamei, S. Itoh, S. Kudoh, Y. Kashino, H. Koike, Red-shifted chlorophyll a bands allow uphill energy transfer to photosystem II reaction centers in an aerial green alga, Prasiola crispa, harvested in Antarctica, Biochim Biophys Acta Bioenerg. 1861 (2020) 148139, https://doi.org/10.1016/j.bbabio.2019.148139.

[11] K. Li, Q. Ye, Q. Li, R. Xia, W. Guo, J. Cheng, Effects of the spatial and spectral distribution of red and blue light on Haematococcus pluvialis growth, Algal Res. 51 (2020) 102045, https://doi.org/10.1016/j.algal.2020.102045.

[12] B.J. Yoder, R.H. Waring, The Normalized Difference Vegetation Index of Small Douglas-Fir Canopies with Varying Chlorophyll Concentrations, Science Inc. 49 (1994) 81-91. 10.1016/0034-4257(94)90061-2.

[13] D. Wang, H. Wang, B. Qian, H. Zou, K. Zheng, X. Zhou, Y. Song, Y. Sheng, Preparation of hydrophobic calcium carbonate phosphors and its application in fluorescent films, J. Lumin. 219 (2020) 116844, https://doi.org/10.1016/j.jlumin.2019.116844.

[14] K.-W. Kim, G.-H. Kim, S.-H. Kwon, H.-I. Yoon, J.-E. Son, J.-H. Choi, Synthesis and photophysical properties of blue-emitting fluorescence dyes derived from naphthalimide derivatives containing a diacetylene linkage group, Dyes Pigment. 158 (2018) 353–361, https://doi.org/10.1016/j.dyepig.2018.05.065.

[15] Z. Zhang, Z. Zhao, Y. Lu, D. Wang, C. Wang, J. Li, One-step synthesis of Eu3+-modified cellulose acetate film and light conversion mechanism, Polymers (Basel). 13 (2020) 113, https://doi.org/10.3390/polym13010113.

[16] D. Hebert, J. Boonekamp, C.H. Parrish 2nd, K. Ramasamy, N.S. Makarov, C. Castaneda, L. Schuddebeurs, H. Mcdaniel, M.R. Bergren, Luminescent quantum dot films improve light use efficiency and crop quality in greenhouse horticulture, Front. Chem. 10 (2022) 988227, https://doi.org/10.3389/fchem.2022.988227.

[17] J. Li, L. Zhangzhong, X. Zhang, X. Wei, S. Zhang, L. Wang, W. Zheng, Effects of light conversion film on the growth of leafy vegetables in facilities under haze weather, Agronomy 12 (2022) 2391, https://doi.org/10.3390/agronomy12102391.

[18] P. Meyer, B. Van De Poel, B. De Coninck, UV-B light and its application potential to reduce disease and pest incidence in crops, Hortic. Res. 8 (2021) 194, https://doi.org/10.1038/s41438-021-00629-5.

[19] S. Shoji, H. Saito, Y. Jitsuyama, K. Tomita, Q. Haoyang, Y. Sakurai, Y. Okazaki, K. Aikawa, Y. Konishi, K. Sasaki, et al., Plant growth acceleration using a transparent Eu3+-painted UV-to-red conversion film, Sci. Rep. 12 (2022) 17155. https://www.nature.com/articles/s41598-022-21427-6.

[20] W. Wu, Z. Zhang, R. Dong, G. Xie, J. Zhou, K. Wu, H. Zhang, Q. Cai, B. Lei, Characterization and properties of a Sr2Si5N8:Eu2+-based light-conversion agricultural film, J. Rare Earths 38 (2020) 539–545, https://doi.org/10.1016/j.jre.2020.01.020.

[21] Y. Wang, Z. Qian, X. Li, A. Qin, Y. Guo, B. Tang, Exploration of high-performance light-conversion agents based on cyanostilbene and phenanthrenecarbonitrile backbones: E/Z and position isomerism, high-contrast Michael addition reaction activity and intramolecular photocyclization, J. Mater. Chem. C 9 (2021) 12681–12693, https://doi.org/10.1039/D1TC02405A.

[22] Y. Liu, Z. Gui, J. Liu, Research progress of light wavelength conversion materials and their applications in functional agricultural films, Polymers (Basel). 14 (2022) 851, https://doi.org/10.3390/polym14050851.

[23] Y. Jiang, C. Yan, H. Zhang, M. Wu, S. Zheng, Y. Zhang, L. Xu, Biodegradable polylactide/rare earth complexes in light conversion agricultural films, Coatings 11 (2021) 139, https://doi.org/10.3390/coatings11020139.

[24] D. Wang, Y. Yu, X. Ai, H. Pan, H. Zhang, L. Dong, Polylactide/poly(butylene adipate-co-terephthalate)/rare earth complexes as biodegradable light conversion agricultural films, Polym. Adv. Technol. 30 (2019) 203–211, https://doi.org/10.1016/j.ijbiomac.2019.01.044Get, rights and content.

[25] Y. Liu, J. Liu, Q. Liu, W. He, I.V. Kityk, Photophysical Spectral Features of fluorescent complexes on the basis of the novel ligand β-thujaplicin, J. Lumin. 218 (2020) 116852, https://doi.org/10.1016/j.jlumin.2019.116852.

[26] Y. Wang, Y. Yu, W. Liu, L. Ren, G. Ge, Exploration of highly efficient blue-violet light conversion agents for an agricultural film based on structure optimization of triphenylacrylonitrile, J. Agric. Food Chem. 66 (2018) 13295–13302, https://doi.org/10.1021/acs.jafc.8b05453.

[27] S. Moi, B. Hosamani, K. Kumar, S. Gunaga, S. Raghothama, K.H. Gowd, Photochemical studies of new synthetic derivatives of avobenzone under sunlight using UV-spectroscopy, J. Photochem. Photobiol. A-Chem. 420 (2021) 113488, https://doi.org/10.1016/j.jphotochem.2021.113488.

[28] H. Zhang, A. Li, G. Li, B. Li, Z. Wang, S. Xu, W. Xu, B.Z. Tang, Achievement of high-performance nondoped blue OLEDs based on AIEgens via construction of effective high-lying charge-transfer state, Adv. Opt. Mater. 8 (2020) 1902195, https://doi.org/10.1002/adom.201902195.

[29] J. Wang, Q. Meng, Y. Yang, S. Zhong, R. Zhang, Y. Fang, Y. Gao, X. Cui, Schiff base aggregation-induced emission luminogens for sensing applications: a review, ACS Sens. 7 (2022) 2521–2536, https://doi.org/10.1021/acssensors.2c01550.

[30] G. Shabir, I. Shafique, A. Saeed, Ultrasound assisted synthesis of 5–7 membered heterocyclic rings in organic molecules, J. Heterocycl. Chem. 59 (2022) 1669–1702, https://doi.org/10.1002/jhet.4527.

[31] A. Keyhani, M. Nikpassand, L.Z. Fekri, H. Kefayati, One-pot synthesis of a new category of 2-aryl-quinazolinones using OImDSA as an efficient heterocyclic medium, Comb. Chem. High Throughput Screen. 25 (2022) 267–273, https://doi.org/10.2174/1386207324999210120194730.

[32] B. Maleki, R. Rooky, E. Rezaei-Seresht, R. Tayebee, One-pot synthesis of bicyclic ortho-aminocarbonitrile and multisubstituted cyclohexa-1,3-dienamine derivatives, Org. Prep. Proced. Int. 49 (2017) 557–567, https://doi.org/10.1080/00304948.2017.1384282.

[33] M. Luo, H.M. Li, One-pot synthesis and biological and catalytic applications of organometallic complexes involving oxazolines and (R)/(S)-a-phenylethylamine, J. Iran. Chem. Soc. 17 (2019) 963–971. https://link.springer.com/article/10.1007/s13738-019-01830-z.

[34] M. Luo, J.C. Zhang, H. Yin, C.M. Wang, S. Morris-Natschke, K.H. Lee, One-step templated synthesis of chiral organometallic salicyloxazoline complexes, BMC Chem. 13 (2019) 51. https://bmcchem.biomedcentral.com/articles/10.1186/s13065-019-0565-z.

[35] M. Luo, J.C. Zhang, W.M. Pang, K.K. Hii, One-step multicomponent synthesis of chiral oxazolinyl-zinc complexes, Chem. Cent. J. 11 (2017) 81. https://bmcchem.biomedcentral.com/articles/10.1186/s13065-017-0315-z.

[36] R. Ramesh, S. Maheswari, S. Murugesan, R. Sandhiya, A. Lalitha, Catalyst-free one-pot synthesis and antioxidant evaluation of highly functionalized novel 1,4-dihydropyridine derivatives, Res. Chem. Intermed. 41 (2014) 8233–8243. https://link.springer.com/article/10.1007/s11164-014-1887-z.

[37] A. Mobinikhaledi, S. Asadbegi, M.A. Bodaghifard, Convenient, multicomponent, one-pot synthesis of highly substituted pyridines under solvent-free conditions, Synth. Commun. 46 (2016) 1605–1611, https://doi.org/10.1080/00397911.2016.1218516.

[38] M. Luo, B. Huang, Z. Xu, S. Liu, Z. Zhu, J. Zhang, X. Meng, Structural investigation, Hirshfeld surface analysis and quantum mechanical study of two dicyanopyridine derivatives, J. Mol. Struct. 1228 (2021) 129748, https://doi.org/10.1016/j.molstruc.2020.129748.

[39] A.A. Amer, Synthesis of some new polyfunctionalized pyridines, J. Heterocycl. Chem. 55 (2018) 297–301. https://onlinelibrary.wiley.com/doi/full/10.1002/jhet.3049.

[40] Y. Qi, Y. Wang, G. Ge, Z. Liu, Y. Yu, M. Xue, Multi-state emission properties and the inherent mechanism of D-A–D type asymmetric organic boron complexes, J. Mater. Chem. C 5 (2017) 11030–11038, https://doi.org/10.1039/C7TC02115A.

[41] M. Huang, H. Lu, K. Wang, B. Liu, M. Wang, X. Qiao, J. Yang, A facile design of azaanthracene derivatives: ACQ–AIE conversion and blue-shifted

mechanofluorochromic emission, Dyes Pigment. 186 (2021) 108992, https://doi.org/10.1016/j.dyepig.2020.108992.
[42] L. Zong, Y. Xie, C. Wang, J.R. Li, Q. Li, Z. Li, From ACQ to AIE: the suppression of the strong pi-pi interaction of naphthalene diimide derivatives through the adjustment of their flexible chains, Chem. Commun Camb. 52 (2016) 11496–11499, https://doi.org/10.1039/C6CC06176A.
[43] F. Ye, C. Shen, J. Guan, Y. Liu, X. Wang, J. Wang, M. Cong, W. Wang, T. Zhang, B. Zou, et al., Facile ACQ-to-AIE transformation via diphenylphosphine (DPP) modification with versatile properties, J. Mater. Chem. C. 10 (2022) 3560–3566, https://doi.org/10.1039/D1TC05810J.
[44] Z. Wang, R. Li, L. Chen, X. Zhai, W. Liu, X. Lin, L. Chen, N. Chen, S. Sun, Z. Li, et al., Precise molecular design of a pair of new regioisomerized fluorophores with opposite fluorescent properties, Front. Chem. 9 (2021) 823519, https://doi.org/10.3389/fchem.2021.823519.
[45] J. Yang, J. Li, P. Hao, F. Qiu, M. Liu, Q. Zhang, D. Shi, Synthesis, optical properties of multi donor–acceptor substituted AIE pyridine derivatives dyes and application for Au3+ detection in aqueous solution, Dyes Pigment. 116 (2015) 97–105, https://doi.org/10.1016/j.dyepig.2015.01.005.
[46] M.T. Cocco, C. Congiu, V. Lilliu, V. Onnis, Synthesis and antiproliferative activity of 2,6-dibenzylamino-3,5-dicyanopyridines on human cancer cell lines, Eur. J. Med. Chem. 40 (2005) 1365–1372, https://doi.org/10.1016/j.ejmech.2005.07.005.
[47] H. Wang, C. Zhao, Z. Burešová, F. Bureš, J. Liu, Cyano-capped molecules: versatile organic materials, J. Mater. Chem. A 11 (2023) 3753–3770, https://doi.org/10.1039/D2TA09699D.
[48] Y. Wang, Q. Liu, Z.C. Zhen, J.L. Liu, R.M. Qiao, W.Q. He, Effects of mica modification with ethylene-vinyl acetate wax on the water vapor barrier and mechanical properties of poly-(butylene adipate-co-terephthalate) nanocomposite films, J. Appl. Polym. 138 (2021) 50610, https://doi.org/10.1002/app.50610.
[49] Y. Ren, Z. Chen, H. Du, L. Fang, X. Zhang, Preparation and evaluation of modified ethylene-vinyl acetate copolymer as pour point depressant and flow improver for Jianghan crude oil, Ind. Eng. Chem. Res. 56 (2017) 11161–11166, https://doi.org/10.1021/acs.iecr.7b02929.
[50] X. Xue, L. Tian, S. Hong, S. Zhang, Y. Wu, Effects of composition and sequence of ethylene-vinyl acetate copolymers on their alcoholysis and oxygen barrier property of alcoholyzed copolymers, Ind. Eng. Chem. Res. 58 (2019) 4125–4136, https://doi.org/10.1021/acs.iecr.8b06260.
[51] Y. He, Y. Wang, X. Li, Y. Guo, L. Ma, Breaking the bottleneck of organic light conversion agents: preparation, performance evaluation and intrinsic mechanism, Spectrochim Acta. Part A: Mol. Biomol. Spectrosc. 288 (2023) 122161, https://doi.org/10.1016/j.saa.2022.122161.
[52] Y. Hu, K. Wang, Y. Wang, L. Ma, Perylene imide derivatives: Structural modification of imide position, aggregation caused quenching mechanism, light-conversion quality and photostability, Dyes Pigment. 210 (2023) 110948, https://doi.org/10.1016/j.dyepig.2022.110948.
[53] I. Osman, DFT study of the structure, reactivity, natural bond orbital and hyperpolarizability of thiazole azo dyes, Int. J. Mol. Sci. 239 (2017) 18, https://doi.org/10.3390/ijms18020239.
[54] Sumit. Patra, Ramalingam. Manivannan, Young-A. Son, Multicolor emissive organic material to display aggregation caused red shift with dual state emission, and application towards rewritable data storage, Acta. Part A: Mol. Biomol. Spectrosc. 444 (2023) 114945. 10.1016/j.jphotochem.2023.114945.
[55] S.E. Jadhav, P.S. Singh, B.R. Madje, S. Chacko, R.M. Kamble, Synthesis, tuning of photophysical and electrochemical properties of Yellow-Red emissive, AIEE active benzamide dyes, Acta. Part A: Mol. Biomol. Spectrosc. 445 (2023) 115085, https://doi.org/10.1016/j.jphotochem.2023.115085.